MBoC | BRIEF REPORT

Tools for live-cell imaging of cytoskeletal and nuclear behavior in the unconventional yeast, *Aureobasidium pullulans*

Claudia A. Petrucco[a], Alex W. Crocker[b], Alec D'Alessandro[a], Edgar M. Medina[c], Olivia Gorman[a], Jessica McNeill[a], Amy S. Gladfelter[d], and Daniel J. Lew[a,†,*]

[a]Department of Pharmacology and Cancer Biology, and [d]Department of Cell Biology, Duke University, Durham, NC 27710; [b]Department of Biochemistry and Biophysics, University of North Carolina, Chapel Hill, NC 27599; [c]Department of Biology, University of Massachusetts, Amherst, MA 01003

ABSTRACT ***Aureobasidium pullulans* is a ubiquitous fungus with a wide variety of morphologies and growth modes including "typical" single-budding yeast, and interestingly, larger multinucleate yeast than can make multiple buds in a single cell cycle. The study of *A. pullulans* promises to uncover novel cell biology, but currently tools are lacking to achieve this goal. Here, we describe initial components of a cell biology toolkit for *A. pullulans*, which is used to express and image fluorescent probes for nuclei as well as components of the cytoskeleton. These tools allowed live-cell imaging of the multinucleate and multibudding cycles, revealing highly synchronous mitoses in multinucleate yeast that occur in a semiopen manner with an intact but permeable nuclear envelope. These findings open the door to using this ubiquitous polyextremotolerant fungus as a model for evolutionary cell biology.**

Monitoring Editor
Sophie Martin
Université de Genève

Received: Oct 10, 2023
Revised: Feb 7, 2024
Accepted: Feb 27, 2024

New Materials

New Methods

SIGNIFICANCE STATEMENT

- The ubiquitous polyextremotolerant fungus *Aureobasidium pullulans* exhibits an unusual and poorly understood multibudding mode of growth, but we lack tools to study its cell biology.
- This work reports the creation of genetically manipulated strains of *A. pullulans* that allow visualization of actin, microtubule, and septin cytoskeletons as well as nuclei and endoplasmic reticulum in live cells.
- Protocols, plasmids, and strains reported here will enable investigation of the novel cell biology of this unconventional yeast.

This article was published online ahead of print in MBoC in Press (http://www.molbiolcell.org/cgi/doi/10.1091/mbc.E23-10-0388) on March 6, 2024.

†Present Address: Biology Department, Massachusetts Institute of Technology, Cambridge, MA 02139

*Address correspondence to: Daniel J. Lew (djlew@mit.edu).

Abbreviations used: AMT, Agrobacterium-mediated transformation; ER, endoplasmic reticulum; NLS, nuclear localization sequence; NPC, nuclear pore complex; T-DNA, transfer-deoxyribonucleic acid.

INTRODUCTION

Our understanding of fundamental cell and developmental biology is largely derived from the study of a small number of tractable model systems. In particular, the budding yeast *Saccharomyces cerevisiae* has revealed conserved molecular pathways underpinning eukaryotic cell biology, from gene expression to protein trafficking to signal transduction and cell-cycle control (Botstein and Fink, 2011). This model organism has also driven our understanding of the life cycles of budding yeasts in general. A conserved cell polarity pathway guarantees formation of a single bud in each cell cycle (Chiou *et al*., 2017). Accurate delivery of one daughter nucleus into the bud is achieved by orienting the mitotic spindle along the

mother-bud axis, and cytokinesis at the mother-bud neck only occurs following properly oriented mitosis (Howell and Lew, 2012). Similar single-bud cell cycles are displayed by a diverse group of yeasts of commercial or medical interest such as *Kluyveromyces lactis* (Schaffrath and Breunig, 2000), *Candida albicans* (Berman, 2006), *Ustilago maydis* (Steinberg and Perez-Martin, 2008), and *Cryptococcus neoformans* (Kopecka *et al*., 2001). However, the simple one bud/one nucleus situation does not encompass the full diversity of budding yeast behaviors. For example, during pulmonary infections of humans, *C. neoformans* yeasts produce titan cells that undergo DNA replication without budding to yield large polyploid cells, which can later bud and divide asymmetrically to make small haploid yeast cells (Gerstein *et al*., 2015; Altamirano *et al*., 2021). Other yeasts, including *Aureobasidium pullulans* (Ramos and Acha, 1975; Mitchison-Field *et al*., 2019; Goshima, 2022), *Paracoccidioides brasiliensis* (Mackinnon and Vinelli, 1949), and *Mucor circinelloides* (Lübbehüsen *et al*., 2003), can make several buds in a single cell cycle, raising the question of how they coordinate the segregation of nuclei and other organelles so that each bud becomes a viable daughter. Understanding these and other unconventional cycles promises to uncover novel mechanisms that, as with much yeast biology, may be applicable in unexpected contexts.

A. pullulans is a ubiquitous black yeast-like fungus with a wide variety of morphologies and growth modes including "typical" single-budding yeast, larger multinucleate yeast that can make multiple buds in a single cell cycle, and multinucleate hyphae with variable morphology (Figure 1A; Ramos and Acha, 1975; Seviour *et al*., 1984). The morphological flexibility may help to explain how it is that *A. pullulans* thrives in a very wide variety of environments, including in soil, in the ocean, and on plants as a saprophyte or endophyte (Slepecky and Stramer, 2009; Gostinčar *et al*., 2014). *A. pullulans* is polyextremotolerant and tolerates cold, acidic, alkaline, and saline environments (Gostinčar *et al*., 2011, 2019). Natural products made by *A. pullulans* have attracted interest from the agriculture and biotechnology industries (Prasongsuk *et al*., 2018), and this yeast produces the cell wall polysaccharide pullulan, which has commercial applications in the food, pharmaceutical, and cosmetic industries (Cheng *et al*., 2011). The recognition that nonmodel organisms constitute a treasure trove of unexamined biology, combined with recent advancements in molecular genetics techniques, has spurred a growing enthusiasm for investigating the cell and developmental biology of nonmodel systems (Gladfelter, 2015; Russel *et al*., 2017). Here, we describe initial components of a cell biology toolkit for *A. pullulans* including methods to express fluorescent probes for nuclei as well as components of the cytoskeleton. Using these tools to image multibudding cycles, we found that *A. pullulans* undergoes a semiopen form of mitosis with an intact but permeable nuclear envelope. Yeast cells formed up to 13 buds in a cell cycle, followed by a mitosis in which all nuclei divided simultaneously so that every bud received at least one nucleus and the mother retained a variable number of nuclei. These behaviors raise problems and questions that did not arise in studies of model yeasts. In doing so, our work challenges assumptions about how cells decide the number of buds to make and how nuclear segregation is managed so as to distribute nuclei to every bud.

RESULTS AND DISCUSSION

As bud formation and nuclear segregation are achieved by appropriate organization of the cytoskeleton, our goal in this work was to develop strains of *A. pullulans* expressing fluorescent proteins that would enable us to track nuclei and cytoskeletal elements in live cells. This would require: (i) an efficient transformation protocol, (ii) genetically encoded fluorophores to enable detection, (iii) promoter sequences directing sufficient expression of tagged probes, and (iv) nonperturbing probes. We chose to work with the strain *A. pullulans EXF-150* isolated from hypersaline waters of Slovenia because its genome had been sequenced, assembled, and annotated (Gostinčar *et al*., 2014). *EXF-150* is easily maintained in the laboratory, and many cells form multiple buds upon culturing in standard YPD media at room temperature (Figure 1A).We tested *EXF-150* for drug sensitivity and found three potential antibiotics for drug selection – hygromycin, nourseothricin, and geneticin (Figure 1B). These were then used as selectable markers for transformation.

Agrobacterium-mediated transformation (AMT) of *A. pullulans*

The phylogeny of *A. pullulans* and its relatives is still being revised, so that some older studies on this species have used different names such as *Pullaria pullulans* (Cooke, 1959) while other studies reporting work on related but distinct species may have called them *A. pullulans* (Onetto *et al*., 2020; Parra *et al*., 2023). We attempted a spheroplast transformation protocol based on reports of success with this method in what was probably *Aureobasidium melanogenum* (Guo *et al*., 2017; Zhang *et al*., 2019), but we were unable to transform our *A. pullulans* isolate with this method. We, therefore, attempted transformation using the plant pathogen *Agrobacterium tumefaciens*, which has been used to transform a variety of organisms (Gelvin, 2003), including *A. pullulans* (Tu *et al*., 2015). *A. tumefaciens* contains a tumor-inducing plasmid with a segment known as the transfer DNA (T-DNA) which is injected into target cells and integrates into the host genome. The T-DNA can be modified to replace the plant tumor induction genes with desired constructs. AMT has been adapted for use in diverse fungi including Ascomycetes, Basidiomycetes, and Mucoromycetes (Idnurm *et al*., 2017). Recently, AMT was used to transform the Chytrid *Spizellomyces punctatus* with a bidirectional histone promoter driving expression of a drug resistance gene and a fluorescent histone H2B (Medina *et al*., 2020). Using plasmids from that study and close derivatives (Table 1), we were able to obtain *A. pullulans* transformants resistant to Hygromycin (HYG) or Nourseothricin (NAT) via AMT. Thus, the control elements in those vectors (*Spizellomyces punctatus [Sp]* histone H2 promoter and *Saccharomyces cerevisiae [Sc] ADH1* terminator) are operational in *A. pullulans*. Drug resistance was stably inherited during asexual proliferation, indicating that constructs had integrated into the *A. pullulans* genome. Transformants exhibited heterogeneous but heritable colony growth rates at different temperatures and heterogenous melanization, suggesting integration of the constructs at different genomic locations (Figure 1C). In all experiments described below, transformants were selected that exhibited no growth defects or colony morphology/melanization differences to the wildtype strain (Figure 1C; Supplemental Figure S1).

Fluorescent tags for live-cell imaging

Imaging of strains expressing fluorescently-tagged *Spizellomyces* histone H2B revealed easily detectable nuclei for tdTomato, mEYFP, and mClover3 tags, but not for GFP, sfGFP, or mNEON tags (Figure 1D). Codon usage analysis revealed that all fluorophores contained similar numbers of *A. pullulans* rare codons (Figure 1E). However, GFP, sfGFP, and mNEON contained multiple TTA codons encoding leucine, while tdTomato had only one, and mEYFP, and mClover3 contained no such codons (Figure 1E). TTA codons can restrict protein production in a context-dependent manner in bacteria (Chater and Chandra, 2008; Silov *et al*., 2021). Thus, we speculate that TTA codon abundance may limit expression of some commonly used fluorescent protein sequences in *A. pullulans*.

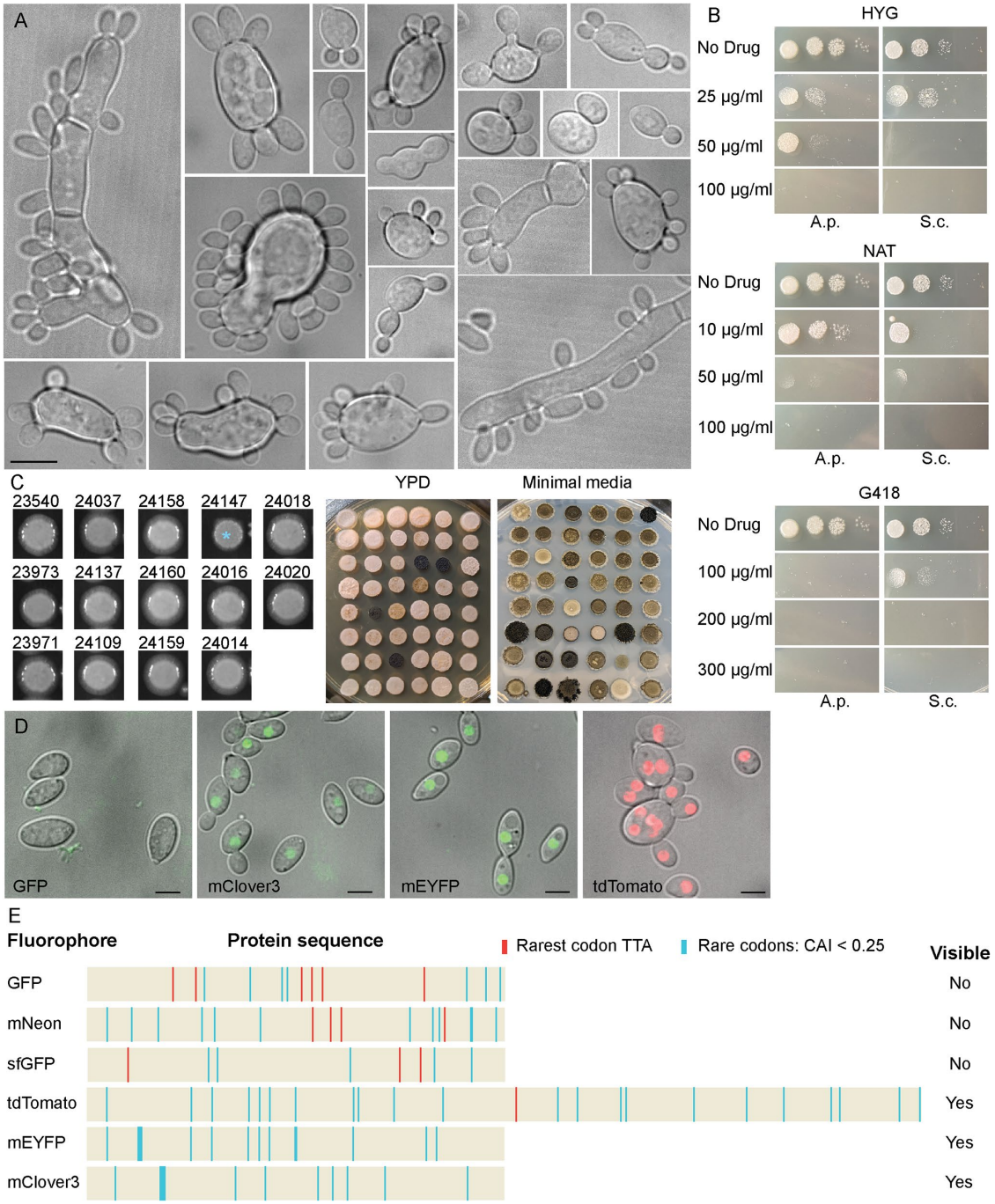

FIGURE 1: *A. pullulans* morphology and transformation. (A) Examples of *A. pullulans* morphology. DIC images of *EXF-150* strain grown in YPD. Scale bar, 10 µm. (B) Sensitivity of *A. pullulans* (A.p.) and *S. cerevisiae* (S.c.) to three antibiotics – hygromycin (HYG), nourseothricin (NAT), and geneticin (G418). 5000, 500, 50, and five cells were spotted onto YPD plates with the indicated antibiotics and grown for 2 d at 25°C. (C) AMT yields antibiotic-resistant colonies. Large colonies behave similarly to the parent untransformed strain (left), with the exception of strains expressing the Lifeact probe from the strong histone promoter (blue asterisk). Numbers correspond to strains used in this study (Table 3). Smaller colonies exhibit a range of morphologies and melanization (right), presumably due to integration of transforming DNA at different genomic locations. The same strains were spotted onto plates with different media as indicated. (D) Transformants with tagged histone H2B show nuclear signal when tagged with mClover3, mEYFP, and tdTomato, but not GFP. Merged DIC and maximum projection images. Scale bar, 5 µm. (E) Presence of *A. pullulans* rare codons (CAI < 0.25) in different fluorescent proteins. TTA codons (orange) were prevalent in genes encoding fluorescent proteins that were not detected.

Visualizing F-actin in *A. pullulans*

As with other fungi (Lichius *et al.*, 2011), the *A. pullulans* genome contains well-conserved cytoskeletal genes implying the presence of actin, microtubule, and septin networks. This includes one each of alpha, beta, and gamma tubulin; a single conventional actin; and the four core septin genes as well as one additional septin. In

Plasmid	Fluorescent probe	Selectable marker	Source
pGI3EM20C	SpH2Bp-H2B-tdTomato	SpH2Ap-Hyg^R	Medina *et al.*, 2020
pGI3EM22C	SpH2Bp-Lifeact-tdTomato	SpH2Ap-Hyg^R	Medina *et al.*, 2020
pDLB 4572	SpH2Bp-H2B-GFP	SpH2Ap-Hyg^R	This study
pDLB 4602	SpH2Bp-H2B-mEYFP	SpH2Ap-Hyg^R	This study
pDLB 4603	SpH2Bp-H2B-mClover3	SpH2Ap-Hyg^R	This study
pDLB 4604	SpH2Bp-NLS-tdTomato	SpH2Ap-Hyg^R	This study
pDLB 4622	ScADH1p-Lifeact-tdTomato	SpH2Ap-Hyg^R	This study
pDLB 4623	ScACT1p-Lifeact-tdTomato	SpH2Ap-Hyg^R	This study
pDLB 4624	ScCYC1p-Lifeact-tdTomato	SpH2Ap-Hyg^R	This study
pDLB 4625	ScTDH3p-Lifeact-tdTomato	SpH2Ap-Hyg^R	This study
pDLB 4640	SpH2Bp-ApNic96-tdTomato	SpH2Ap-Hyg^R	This study
pDLB 4650	ScACT1p-ApTub4-tdTomato	SpH2Ap-Hyg^R	This study
pDLB 4651	ScACT1p-ApSec61-tdTomato	SpH2Ap-Hyg^R	This study
pDLB 4668	ScACT1p-ApBim1-tdTomato	SpH2Ap-Hyg^R	This study
pDLB 4677	ScACT1p-ApCdc3-tdTomato	SpH2Ap-Hyg^R	This study
pDLB 4678	ScACT1p-ApCdc11-tdTomato	SpH2Ap-Hyg^R	This study
pDLB 4679	ScACT1p-ApCdc10-tdTomato	SpH2Ap-Hyg^R	This study
pDLB 4686	SpH2Bp-H2B-mEYFP	SpH2Ap-Nat^R	This study

TABLE 1: Plasmids used in this study.

S. cerevisiae, all of these cytoskeletal elements contribute to accurate segregation of nuclei and other organelles into the bud. To visualize these networks, we developed constructs to tag relevant proteins with tdTomato. We began by utilizing Lifeact (Riedl *et al.*, 2008), a short F-actin-binding peptide consisting of the first 17 amino acids of *S. cerevisiae* Abp140, to visualize F-actin. We obtained multiple transformants expressing Lifeact-tdTomato from the *Spizellomyces* histone promoter. However, unlike transformants expressing nuclear probes, transformants expressing Lifeact-tdTomato all exhibited growth defects and a frequent failure of buds to detach from the mother cell (Figure 2A). As actin is important for fungal cytokinesis (Walther and Wendland, 2003), this raised the possibility that high-level expression of Lifeact from the histone promoter interfered with actin function in cytokinesis. Previous studies have documented that high-level Lifeact expression can induce aberrant actin structures including thick bundles that can form loops and lariats (Courtemanche *et al.*, 2016). Similar structures were readily observed in *A. pullulans* transformants (Figure 2A), suggesting that the high levels of Lifeact expressed from the histone promoter were interfering with proper actin organization in *A. pullulans*.

To express Lifeact-tdTomato at lower levels, we tested four promoters from *S. cerevisiae* (Sc*TDH3*, Sc*ACT1*, Sc*ADH1*, and Sc*CYC1*) known to exhibit differing levels of expression. Transformants with these promoters driving Lifeact no longer had buds failing to detach from the mother cell (Figure 2B). Western blotting indicated that transformants with the Sp*H2B*, Sc*ACT1*, Sc*ADH1*, Sc*CYC1*, and Sc*TDH3* promoters expressed decreasing amounts of Lifeact-tdTomato (Figure 2C). This finding suggests that *S. cerevisiae* promoters are functional in *A. pullulans*, although resulting expression levels in this context did not reflect the strength of these promoters in *S. cerevisiae*, where *TDH3* is the strongest (Xiong *et al.*, 2018). Imaging results were consistent with the expression levels indicated by the western blot data, and none of the new transformants displayed the growth defects that were observed in the initial histone-promoter-driven Lifeact. Instead, Lifeact labeled linear structures (presumed cables) extending from the bud into the mother, as well as cortical patches, and, in cells with larger buds, presumed cytokinetic rings at the mother-bud neck (Figure 2B). These results suggest that *A. pullulans* generates actin cables, patches, and rings analogous to those described in other fungi. These Lifeact-tdTomato-decorated structures disappeared following 15-min treatment with 200 µM Latrunculin A (Figure 2D), supporting the idea that they represent F-actin cables and patches. Some treated cells developed a dark comet-like object, whose nature remains unknown (Figure 2D). Based on the results with Lifeact-tdTomato, we expressed most other cytoskeleton-related probes from the Sc*ACT1* promoter to avoid potential overexpression artefacts.

Visualizing microtubule ends in *A. pullulans*

We next set out to visualize microtubules by tagging *A. pullulans* α-tubulin (Ap*TUB1*) and β-tubulin (Ap*TUB2*), but initial attempts with N- and C- terminal tdTomato tags were unsuccessful. As an alternative, we tagged *A. pullulans* proteins expected to decorate either the microtubule minus end (γ-tubulin Ap*TUB4*) or plus end (EB1 homologue Ap*BIM1*). These probes did reveal fluorescent signals consistent with spindle pole bodies (SPBs: Tub4-tdTomato; Figure 3A) and microtubule plus ends (Bim1-tdTomato; Figure 3, B and D). During mitosis, strong Tub4 puncta (presumed SPBs) duplicated and then moved apart (Figure 3A). Imaging using increased illumination revealed fainter Tub4-tdTomato puncta of varied size and intensity in nonmitotic cells (Figure 3C). This could be indicative of interphase microtubule organizing centers (MTOCs) aside from SPBs, which have been described in several other fungi (Straube *et al.*, 2003; Sawin *et al.*, 2004; Konzack *et al.*, 2005; Sutradhar *et al.*, 2015). During mitosis, Bim1 puncta condensed into a bar-like structure (presumed mitotic spindle) that elongated rapidly and then disappeared, leaving behind two puncta (Figure 3B). Individual microtubule plus ends were not clearly discerned, but fainter

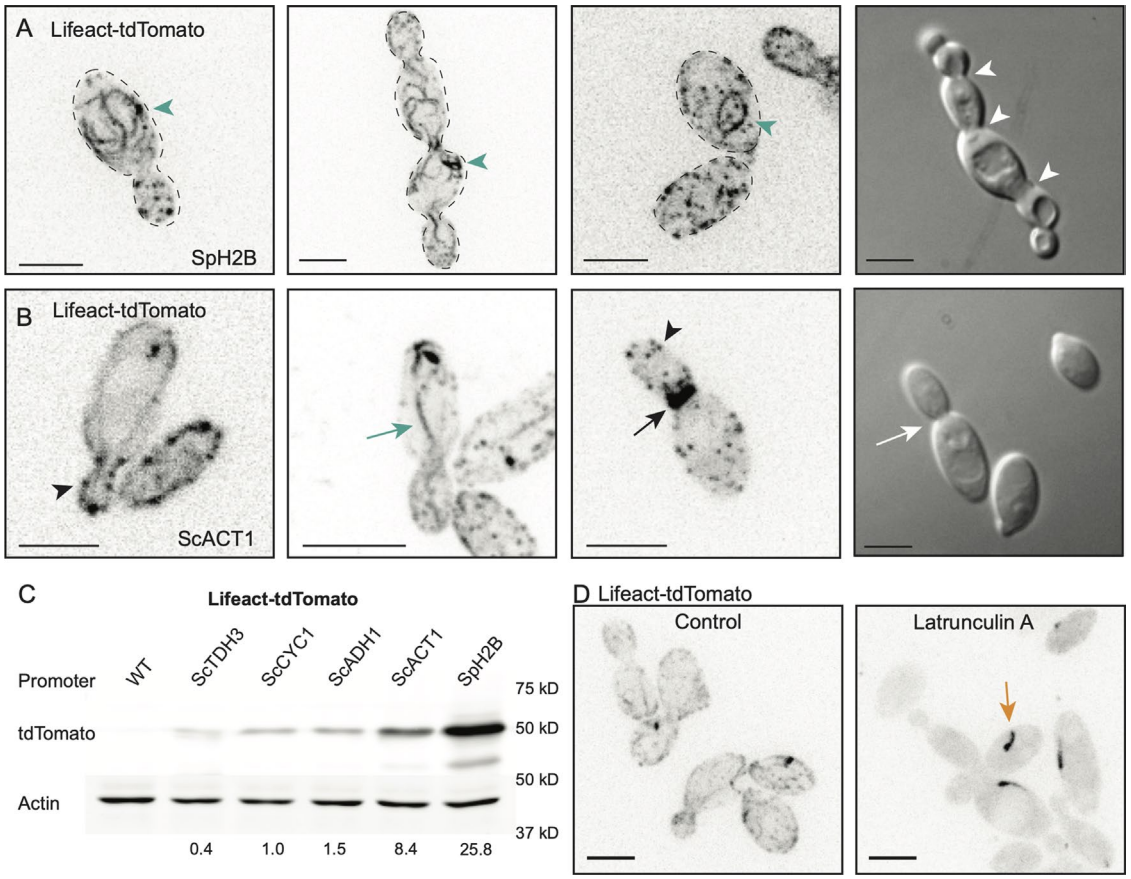

FIGURE 2: Visualization of F-actin in *A. pullulans*. (A) Lifeact-tdTomato expressed from the SpH2B promoter decorates cytoplasmic loops and lariats (green arrowheads), and buds from these cells often fail to divide and detach from mother cell (white arrowheads indicate sites of failed cytokinesis). Inverted maximum projection and DIC images of DLY24147. (B) F-actin structures in cells expressing Lifeact-tdTomato from the ScACT1 promoter, highlighting examples of cortical actin patches (black arrowheads), actin cables extending from mother to bud (green arrow), and putative rings at the mother-bud neck (black arrow). Buds did not fail to detach from mother cells (white arrows indicate normal cytokinesis). Inverted maximum projection and DIC images of DLY24016. (C) Western blot of Lifeact-tdTomato expressed from different promoters in *A. pullulans*. Cell extracts were analyzed by western blotting with antibodies against tdTomato and actin. tdTomato abundance (normalized against actin) is shown below each lane. Similar results were obtained in two western blots. Strains DLY23540, DLY24020, DLY24018, DLY24014, DLY24016, and DLY24147. (D) Treatment of cells expressing Lifeact-tdTomato with 200 µM Latrunculin A for 15 min eliminated all cables and patches but not an occasional dark comet (orange arrow). Inverted maximum projection images of DLY24016. Scale bars, 5 µm.

Bim1-tdTomato puncta were detected upon imaging with increased illumination, even in cells that lacked obvious spindles (Figure 3D). Most Bim1-tdTomato-decorated structures disappeared following 15-min treatment with microtubule polymerization inhibitors Nocodazole (50 nM) or Benomyl (200 µM), supporting the idea that they represent microtubule ends (Figure 3E).

Visualizing septins in *A. pullulans*

To visualize septins, we tagged three core septin genes (Ap*CDC3*, Ap*CDC10*, and Ap*CDC11*) with tdTomato. Cdc3, Cdc10, and Cdc11 probes concentrated at the mother-bud necks of small and large buds (Figure 3F; Supplemental Figure S2). These three septins also labeled linear elements and rows of puncta at the cell cortex in unbudded cells. In aggregate, these observations indicate that *A. pullulans* exhibits the polarized actin cytoskeleton, microtubule spindle, and cortical septin structures at the neck that are typical of *S. cerevisiae* and other well-studied budding yeasts (Gladfelter *et al.*, 2001; Warenda and Konopka, 2002; Kozubowski and Heitman, 2010).

Synchronous mitosis in *A. pullulans*

Previous work demonstrated that many *A. pullulans* cells are multinucleated (Mitchison-Field *et al.*, 2019). To assess the degree to which mitosis in such cells occurred synchronously, we imaged cells expressing H2B-tdTomato. In interphase, the H2B signal appeared to occupy a cup-shaped volume (Figure 4A). During mitosis the H2B signal became more condensed in a presumed metaphase plate, and then underwent a rapid segregation to mother and buds (Figure 4C; Supplemental Movie 1). We used the area of high H2B pixel intensity (with a suitable geometric correction factor upon division of one signal into two: Figure 4B) as a proxy for chromatin condensation and subsequent decondensation (Figure 4C). In mononucleate cells, the average duration of mitosis was 7.4 ± 1.5 min (mean ± SD; n = 58; Figure 4D). This is somewhat more rapid than mitosis in *S. cerevisiae*, where anaphase duration is ~15 min (Yang *et al.*, 1997). In multinucleated cells, mitosis appeared very synchronous, with all nuclei condensing within 30 s of each other (n = 65; Figure 4E).

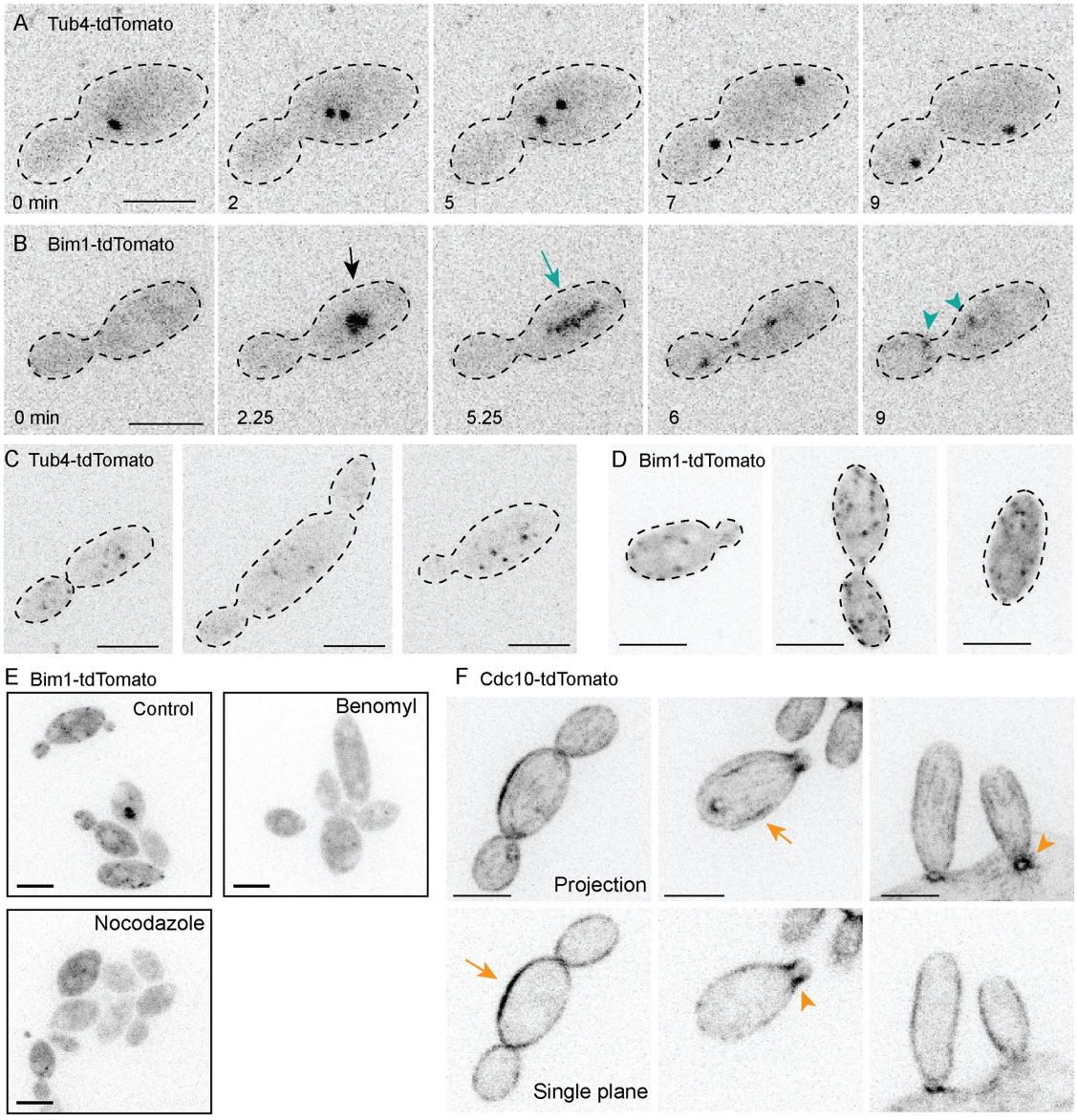

FIGURE 3: Visualization of microtubule ends and septins in *A. pullulans*. (A) Dividing cells show strong Tub4-tdTomato puncta consistent with separating SPBs in mitosis. Time-lapse inverted maximum projection images of DLY24109. (B) Dividing cells show a strong Bim1-tdTomato signal (black arrow) that elongates (green arrow) and disassembles leaving two puncta (green arrowheads) in a manner suggestive of mitotic spindle behavior. Time lapse inverted maximum projection images of DLY24137. (C) Some postmitotic cells exhibit multiple faint Tub4-tdTomato puncta (potential non-SPB MTOCs). Inverted maximum projection images of DLY24019 taken with stronger illumination. (D) Some postmitotic cells exhibit multiple weak puncta of Bim1-tdTomato consistent with interphase microtubule plus ends. Inverted maximum projection images of DLY24137 taken with stronger illumination. (E) Cells expressing Bim1-tdTomato were treated with 50 nM Nocodazole or 200 µM Benomyl for 15 min. Treated cells had few Bim1-tdTomato puncta and lacked presumed mitotic spindles. Inverted maximum projection images of DLY24137. (F) Septin probe Cdc10-tdTomato. Postmitotic cells exhibit fainter linear cortical elements (orange arrows). Dividing cells show a strong septin signal at each mother-bud neck (orange arrowheads). Inverted maximum projection (top) and single-plane (bottom) confocal images of DLY24160. Scale bars, 5 µm.

Semiopen mitosis in *A. pullulans*

Animal cells undergo an "open" mitosis during which the nuclear envelope breaks down, whereas several yeasts including *S. cerevisiae* undergo a "closed" mitosis with an intact nuclear envelope throughout the process. Other fungi exhibit "semiopen" variations of mitosis in which the nuclear envelope is partially broken down (Theisen *et al.*, 2008; Aoki *et al.*, 2011), or the nuclear envelope remains intact, but nuclear pore complexes (NPCs) become permeable due to loss of some NPC components (De Souza *et al.*, 2004).

In *A. pullulans*, a fluorescent protein fused to a nuclear localization sequence (NLS) accumulated in the nucleus during interphase but dispersed throughout the cytoplasm during mitosis (Figure 5A; Supplemental Movie 2). This contrasts with the behavior of such reporters in *S. cerevisiae*, where the fluorescent signal remains enriched in the nucleus throughout the cell cycle (Durandau *et al.*, 2015). In *A. pullulans*, the NLS probe was excluded from nuclei for 9.4 ± 1.1 min (mean ± SD; $n = 50$; Figure 5B). This is ~2 min longer than the interval during which the H2B signal was condensed (Figure 4D), suggesting

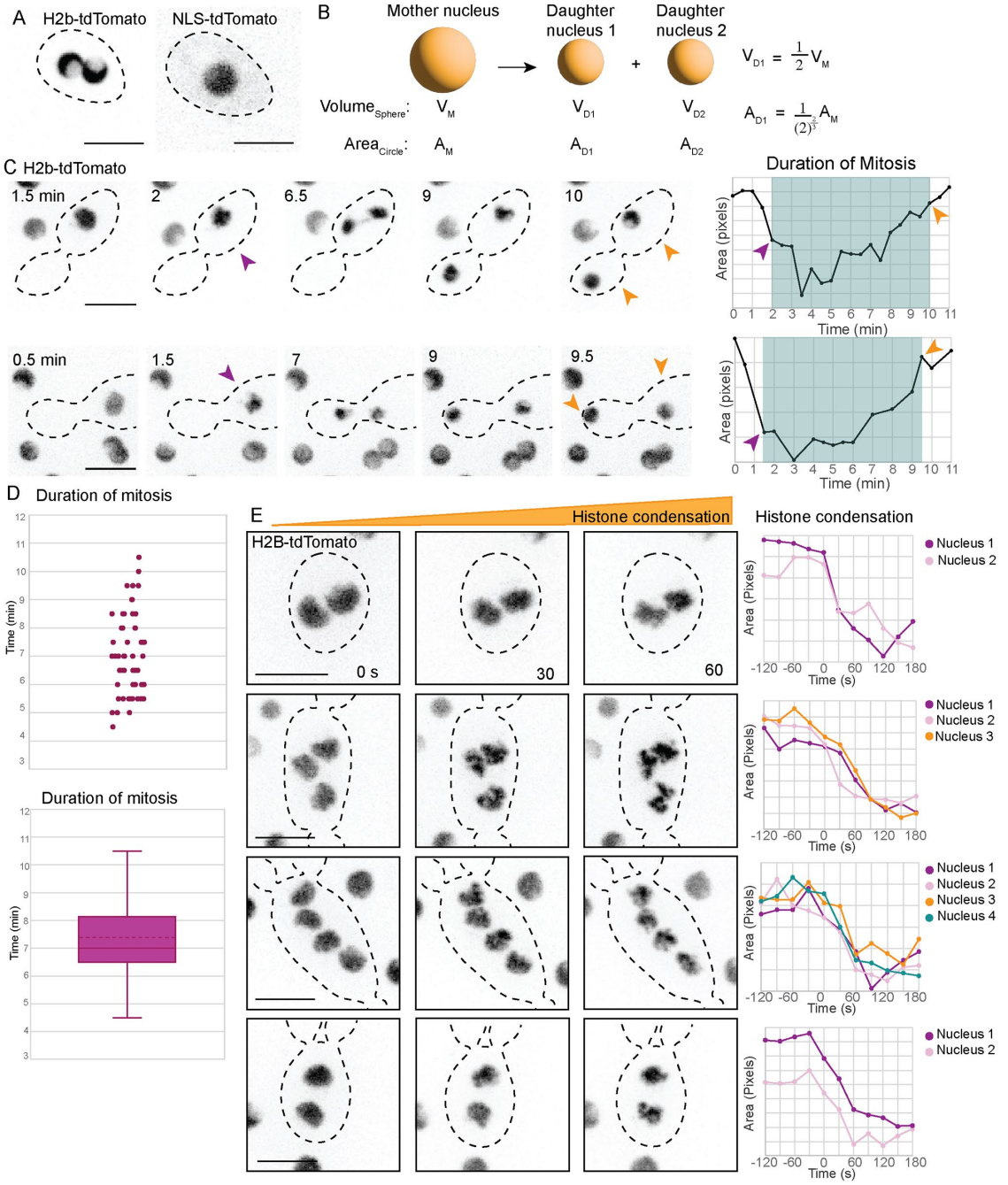

FIGURE 4: Synchronous mitosis in *A. pullulans*. (A) H2B-tdTomato signal (presumed chromatin) decorates a cup-shaped zone in interphase cells, in contrast to NLS-tdTomato that appears as uniform spheres (presumed nuclei). Inverted single plane confocal images of DLY23973 and DLY23971. (B) When a sphere is divided into two spheres with preservation of total volume (presumed condition for division of a mother nucleus into daughter nuclei), the summed areas of the daughter spheres are greater than the area of the mother sphere, and a geometrical correction factor is used to plot area. (C) Time-lapse images of H2B-tdTomato signal reveal a rapid mitosis whose duration can be measured from condensation (purple arrowhead) to decondensation (orange arrowhead). Line graphs plot area of H2B-tdTomato signal: condensation results in decreased area. Mitosis is indicated by the blue box. (D) Scatter plot and box-and-whiskers plot of the duration of mitosis measured as in (C) ($n = 58$ cells). Dotted line is the mean. (E) H2B-tdTomato signals condense synchronously in multinucleated cells. Time lapse inverted maximum projection images taken at 30-s intervals. Line graphs plot the area of each H2B-tdTomato nucleus leading up to and following the start of mitosis. Nuclei in the same cell condense at the same time. Scale bars, 5 μm.

that nuclear permeabilization may precede chromatin condensation, or continue after chromatin decondensation (or both). Tagging of the nuclear envelope/ER protein Sec61 revealed an ER network including the nuclear envelope (Figure 5C). The nuclear envelope appeared to remain intact during mitosis, deforming into two and then three lobes before dividing (Figure 5D; Supplemental Movie 3). This is similar to what has been described in *Aspergillus nidulans*, where the three lobes include two daughter nuclei and a central

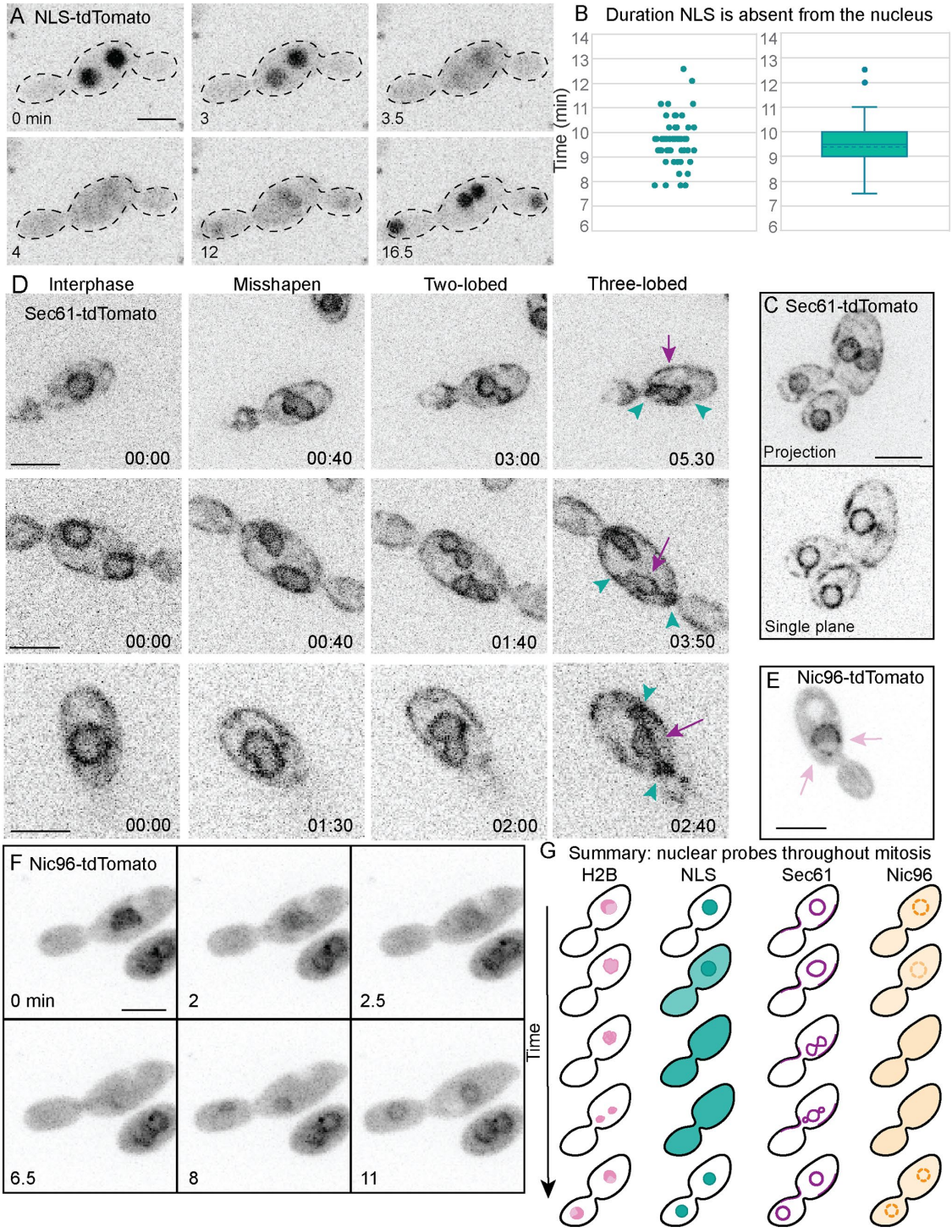

FIGURE 5: Semiopen mitosis in *A. pullulans*. (A) NLS-tdTomato signal disperses during mitosis. Inverted maximum projection image time-lapse series of DLY23971. (B) Scatter plot and box-and-whiskers plot of the interval during which the NLS probe was dispersed (dotted line is mean; $n = 50$ cells). (C) Sec61-tdTomato (presumed ER) decorates both cortical and perinuclear regions. Inverted maximum projection (top) and single-plane (bottom) images of DLY24037. (D) During mitosis Sec61-tdTomato (presumed nuclear envelope) progresses from a circle to a misshapen ovoid, then two-lobed and three-lobed intermediates before resolving to two daughter circles. In the three-lobed intermediates the lobe in the middle (purple arrow) was larger than the other two (green arrowheads). Inverted maximum projection image time-lapse series of DLY24037. (E) Nic96-tdTomato decorates puncta (presumed nuclear pore complexes) around a sphere in interphase (pink arrows). Inverted single plane images of DLY24031. (F) Nic96-tdTomato signal dissipates during mitosis. Inverted maximum projection image time-lapse series of DLY24031. Scale bars, 5 μm. (G) Summary and interpretation. Before chromosome condensation, nuclear pores become permeable, with dispersal of Nic96 and NLS probes from the nucleus. The chromatin (histone signal) then condenses, and the envelope (Sec61 signal) deforms to generate separate daughter nuclei. Following chromosome decondensation, the nuclear pores resume transport and the NLS probe reconcentrates in the nuclei.

nucleolar remnant that disperses (Ukil *et al.*, 2009). In *A. nidulans*, a subset of nuclear pore complex proteins disperses during mitosis leading to a permeable nuclear envelope (De Souza *et al.*, 2004). Tagging of the NPC component Nic96 (Grandi *et al.*, 1993) revealed multiple puncta around a sphere, presumably the nucleus, during interphase (Figure 5E). During mitosis, Nic96-tdTomato was largely dispersed into the cytoplasm (Figure 5F; Supplemental Movie 4). We infer that during mitosis in *A. pullulans,* the nuclei become permeable due to the disassembly of at least a portion of the NPCs. In summary, *A. pullulans* undergoes a form of "semiopen" mitosis where the nuclear pores become permeable, the chromosomes condense, and the nuclear envelope deforms to generate two daughter nuclei (Figure 5G).

CONCLUSION

The protocols, reagents, and strains reported here provide tools to allow high resolution observations and perturbation of cell behaviors in *A. pullulans.* The ability of *A. pullulans* to generate multiple buds simultaneously within a single cell cycle raises new questions about fungal cell biology. In particular, it is unclear how cell polarity is regulated to yield the specific number of buds made by each cell, or how the cytoplasm, membranes, nuclei and organelles made by the mother cell are divided among its various buds. In addition, the morphologic diversity of this fungus and its ability to tolerate many extreme environments raises other fascinating questions that will also become susceptible to molecular genetics and cell biological investigation as the initial toolkit described here expands.

MATERIALS AND METHODS

Request a protocol through *Bio-protocol.*

Plasmids and *A. pullulans* strains

Plasmids used in this study are listed in Table 1. All plasmids and plasmid sequences are available upon request. Plasmids pGI3EM20C and pGI3EM22C for AMT were previously reported (Medina *et al.*, 2020; Table 1). They consist of a pGI3 backbone (Ianiri *et al.*, 2017) that has replication origins and selectable markers (Kan^R and *URA3*) for *Escherichia coli* and *S. cerevisiae*, and a T-DNA insertion region with the Hyg^R selectable marker and fluorescent probes divergently expressed from the *Spizellomyces punctatus* (hereafter Sp) bidirectional histone 2A/2B promoter. Plasmids used in this study were constructed by modifying the T-DNA insertion region of pGI3EM20C or pGI3EM22C.

Molecular biology protocols for standard cloning reactions and In-fusion assembly (Takara Bio USA) followed manufacturer's recommendations.

To tag histone H2B with different fluorophores, we first digested pGI3EM20C with *Bam*H1 and *Pme*I to excise tdTomato and terminator sequences, and restored the *ADH1* terminator by In-fusion assembly with primers that introduced unique *Bam*HI and *Sac*I sites between the H2B and terminator sequences. This intermediate plasmid (pDLB4565) was digested with *Bam*HI and *Sac*I and used as a backbone to clone PCR products generated with primers introducing appropriate restriction sites, encoding GFP (pDLB4572), mEYFP (pDLB4602), and mClover3 (pDLB4603). Correct C-terminal fusion to H2B was confirmed by sequencing.

To generate a probe for the nucleus, we digested pGI3EM20C with *Bam*H1 and *Sal*I to excise H2B coding sequences, and cloned in an NLS-containing fragment by In-fusion assembly, yielding pDLB4604. The NLS fragment is derived from a MAPK biosensor carrying two tandem NLS sequences and MAPK docking sites (Durandau *et al.*, 2015). That sensor was developed to allow export of the probe upon phosphorylation, but we used a mutant version that cannot be phosphorylated, and is constitutively nuclear in *S. cerevisiae*.

To express Lifeact-tdTomato at different levels, we first digested pGI3EM22C with *Pac*I and *Sal*I to excise the bidirectional histone promoter upstream of Lifeact-tdTomato, and cloned in a truncated version retaining the H2A promoter to drive Hygromycin resistance marker but replacing the H2B promoter with a *Kpn*I site. This intermediate plasmid (pDLB4620) was digested with *Kpn*I and *Sal*I and used as a backbone to clone PCR products generated with primers introducing appropriate restriction sites, to insert *S. cerevisiae ADH1* (pDLB4622), *ACT1* (pDLB4623), *CYC1* (pDLB4624), and *TDH3* (pDLB4625) promoters upstream of Lifeact-tdTomato.

A. pullulans homologues of *S. cerevisiae* genes were uncovered by first identifying the Pfam domain(s) present in the protein of the *S. cerevisiae* gene using *Saccharomyces* Genome Database (SGD) and then identifying the protein in *A. pullulans EXF-150* with the same domain using JGI MycoCosm. If more than one protein had the domain, as is the case for the septin proteins, those protein sequences were compared with the *S. cerevisiae* gene via BLAST. *A. pullulans* protein IDs are listed in Table 2. homologues are designated by the *S. cerevisiae* gene name preceded by Ap. In all cases *A. pullulans* genes were amplified by PCR from *EXF-150* genomic DNA from the start codon to the stop codon, and therefore, retain any intron sequences.

To express ApNic96-tdTomato from the H2B promoter, we first digested pGI3EM22C with *Bam*H1 and *Sal*I to excise Lifeact, and cloned a ApNIC96 PCR fragment in its place using In-fusion assembly, yielding pDLB4640.

To express ApSec61, ApTub4, or ApBim1 from the ScACT1 promoter, we first digested pGI3EM22C with *Sal*I and *Bam*H1 to excise Lifeact and cloned ApSEC61, ApTUB4, or ApBIM1 PCR fragments in its place using Infusion assembly. These plasmids drive expression from the strong histone promoter. To replace that with the moderate ScACT1 promoter, plasmids were digested with *Pac*I and *Sal*I to excise the bidirectional histone promoter, and ScACT1p was

S. cerevisiae protein	Pfam domain	Pfam description	*A. pullulans* protein ID
Nic96	PF04097	Nucleoporin interacting component Nup93/Nic96	289161
Sec61	PF00344	SecY/SEC61-alpha family	345851
Tub4	PF00091	Tubulin/FtsZ family, GTPase domain	37813
Bim1	PF03271	EB1, C-terminal	345735
Cdc3	PF00735	Septin-type guanine nucleotide-binding (G) domain	275598
Cdc10	PF00735	Septin-type guanine nucleotide-binding (G) domain	342729
Cdc11	PF00735	Septin-type guanine nucleotide-binding (G) domain	354011

TABLE 2: *A. pullulans* homologues of *S. cerevisiae* genes used in this study.

Strain	Genotype	Source
DLY 23540	Wildtype *EXF-150*	Gostinčar *et al.*, 2014
DLY 23967	SpH2ABp-H2B-meYFP: Hyg^R	This study
DLY 23969	SpH2ABp-H2B-mClover3: Hyg^R	This study
DLY 23971	SpH2ABp -NLS-tdTomato: Hyg^R	This study
DLY 23973	SpH2ABp-H2B-tdTomato: Hyg^R	This study
DLY 24014	ScADH1p-Lifeact-tdTomato: Hyg^R	This study
DLY 24016	ScACT1p-Lifeact-tdTomato: Hyg^R	This study
DLY 24018	ScCYC1p-Lifeact-tdTomato: Hyg^R	This study
DLY 24020	ScTDH3p-Lifeact-tdTomato: Hyg^R	This study
DLY 24031	SpH2ABp-Nic96-tdTomato: Hyg^R	This study
DLY 24037	ScACT1p-Sec61-tdTomato: Hyg^R	This study
DLY 24109	ScACT1p-Tub4-tdTomato: Hyg^R	This study
DLY 24137	ScACT1p-Bim1-tdTomato: Hyg^R	This study
DLY 24147	ScACT1p-Lifeact-tdTomato: Hyg^R	This study
DLY 24158	ScACT1p-Cdc3-tdTomato: Hyg^R	This study
DLY 24159	ScACT1p-Cdc11-tdTomato: Hyg^R	This study
DLY 24160	ScACT1p-Cdc10-tdTomato: Hyg^R	This study
DLY 24161	SpH2ABp-H2B-meYFP: Nat^R	This study

TABLE 3: Yeast strains used in this study.

amplified by PCR from pDLB4623 template, digested with *Pac*I and *Sal*I, and cloned into the corresponding sites by ligation, yielding pDLB4651, pDLB4650, and pDLB4668.

To express ApCdc3, ApCdc10, or ApCdc11 from the ScACT1 promoter, we first generated an intermediate plasmid from pDLB4623 that replaced Lifeact with cloning sites *Spe*I and *Bam*HI (pDLB4674). ApCdc3, ApCdc10, or ApCdc11 genomic fragments were amplified by PCR with primers carrying *Spe*I and *Bam*HI sites, and cloned into the corresponding sites in pDLB4674 by ligation, yielding pDLB4677-9.

A. pullulans strains used in this study are listed in Table 3. All strains are available upon request. Strains were generated by AMT of strain *EXF-150*, with transformants selected that did not show colony morphology or growth phenotypes. Insertion points of the T-DNA in the genome have not been mapped.

Growth and transformation of *A. pullulans*

We used *Aureobasidium pullulans EXF-150* (Gostinčar *et al.*, 2014) and derivatives for all experiments. *A. pullulans* was grown at 24°C in YPD medium (2% dextrose [Sigma], 2% bacto-peptone [Life Technologies], 1% yeast extract [Life Technologies], and for plates 2% bacto-agar [Life Technologies]).

Competent *A. tumefaciens* strain EHA105 was prepared following the protocol from (Medina *et al.*, 2020) and plasmids were transformed into competent bacteria using 0.1 cm cuvettes in a Gene Pulser electroporator (BioRad) at 250 µFD, 200 Ω, 1.8 kV. Transformants were prepared for coincubation according to (Medina *et al.*, 2020).

A. pullulans cells were grown overnight at 24°C in YPD medium to saturation. These mostly small mononucleate cells were washed in IM media, (Minimal Media salts, 40 mM 2-(N-morpholino)ethanesulfonic acid [MES] pH 5.3, 10 mM glucose, 0.5% [wt/vol] glycerol, 200 µM acetosyringone; Bundock *et al.*, 1995). Minimal Media salts contain 11.77 mM K_2HPO_4, 10.6 mM KH_2PO_4, 2.57 mM NaCl, 2.03 mM $MgSO_4$, 0.46 mM $CaCl_2$, 9 nM $FeSO_4$, and 3.78 mM $(NH_4)_2SO_4$ (Hooykaas *et al.*, 1979). Washed cells were diluted to an OD_{600} of 0.5.

Yeast, bacteria, and IM media were combined to a ratio of 1:2:1 in a final volume of 200 µl on IM plates (IM media with 2% agar) as described in (Medina *et al.*, 2020) and incubated for 3 d at room temperature. After coincubation, 2 ml of YPD were added, cells were collected with a cell scraper and pelleted by centrifugation at 3400 g for 8 min. Pellets were resuspended in 200 µl YPD and spread on YPD plates containing 50 mg/l Carbenicillin (Invitrogen) and 50 mg/l Tetracycline (Sigma) to select against *Agrobacterium* and 200 mg/l Hygromycin B (Sigma) or 200 mg/l Nourseothricin (VWR Chemicals) to select for *A. pullulans* transformants. Transformation plates were incubated at 24°C, and colonies were evident within 3–4 d. When transforming a fluorescent probe, around 80% of drug-resistant colonies showed fluorescence.

To ensure the growth and colony morphology of transformed strains was consistent with that of untransformed *EXF-150*, 5000, 500, 50, and five cells were spotted onto the same YPD plate and incubated for 2 d at 24°C

Microscopy

Cells were grown overnight at 24°C in YPD and mounted on slabs containing complete synthetic medium (CSM; 2% dextrose, 0.7% yeast nitrogen base without amino acids, and 0.08% complete supplement mixture; Bio 101) solidified with 2% agarose (VWR Chemicals). All imaging experiments were conducted at room temperature (22–25°C).

Images were acquired with an Andor Revolution XD spinning-disk confocal microscope (Andor Technology) with a CSU-X1 5000-rpm confocal scanner unit (Yokogawa) and a UPLSAPO 100 ×/1.4 oil-immersion objective (Olympus) controlled by MetaMorph software (Molecular Devices). Some time-lapse images were taken with a UPLSAPO 60x/1.3 silicon oil objective. Images were captured by an iXon 897 EMCCD camera (Andor Technology) or an iXon Life 888 EMCCD camera (Andor Technology).

Some DIC images were acquired with a Zeiss Axio Observer Z1 with a 100x/1.3 oil Plan-NEOFLUAR objective (Carl Zeiss Microscopy) controlled by MetaMorph software (Molecular Devices). Images were captured by a photometrics evolve back-thinned EM-CCD camera (Teledyne Photometrics).

Z stacks with 17 z steps of 0.25 or 0.5 µm were acquired at intervals between 10 s and 1 min. Exposure time was 200 ms.

At least three independent movies were collected for each strain.

Image Analysis

To score mitosis duration and synchronicity of mitosis by histone condensation, the area of the H2B-tdTomato signal of a max-projection image was measured over time. Mitosis was defined as the time when the area of H2B-tdTomato signal dramatically decreased, coinciding with the condensation of histones, to when the corrected area of the two daughter nuclei reached the premitotic mother nucleus's area. When the volume of a sphere is halved (presumably what happens when a nucleus divides) each daughter nucleus has half the volume of the mother, so the projected cross-sectional area of each daughter nucleus is more than half the area of the mother. To plot the area so that the summed areas of the daughter nuclei would reflect the area of the mother nucleus we applied a geometrical correction factor of 0.63.

To score the interval during which the NLS probe was dispersed from the nucleus, we visually scored each maximum projection image as nuclear or dispersed.

Codon Usage

The codon preferences in *EXF-150* were evaluated by calculating the codon adaptation index (CAI) for each codon (Sharp and Li, 1987) based on the coding sequences of all genes. Coding sequences were downloaded from NCBI (GenBank GCA_000721785.1). Calculation of CAI was performed using Python and the Biopython (Cock *et al*., 2009) module SeqUtils. Visualizations were made using Matplotlib (Hunter, 2007).

Western blots

Cells were grown overnight in YPD to saturation and then back diluted to an OD_{600} of 0.1 and allowed to grow for 4 h. Cells were pelleted via centrifugation, media was removed, and pellets were stored on ice. Pellets were resuspended in cold lysis buffer (8M urea, 75 mM NaCl, 50 mM Tris-HCl, pH 8.0, 50 mM NaF, 2 mM PMSF, 1X Halt protease and phosphatase inhibitor cocktail [Pierce 78445]) and an equal volume of ice-cold 0.5-mm glass beads was added to each sample. Cells were bead beaten in the cold using a Labnet Vortex Mixer (S0200) at maximum speed for 10 min. Supernatant was removed and mixed with sample buffer (125 mM Tris-HCl, pH 6.8, 4% SDS, 30% glycerol, 0.05% bromophenol blue, 200 mM DTT). Samples were boiled for 5 min, then centrifuged at 21,000 xg for 5 min to pellet any insoluble material. Samples were run on a 10% SDS-polyacrylamide gel and blotted to nitrocellulose overnight at 30V using Towbin buffer (20% MeOH, 25 mM Tris, 192 mM glycine). Blots were dried, then rehydrated, and blocked with 3% milk. Blots were stained with mouse monoclonal anti-tdTomato (OTI2H2; OriGene) or mouse monoclonal antiactin (C4; MP Biomedicals).

ACKNOWLEDGMENTS

We thank Alison Wirshing, Audrey Williams, Erin Curtis, and Corrina Robertson for comments on the manuscript. Imaging was performed with instruments of the Duke Light Microscopy Core Facility, and we thank Lisa Cameron and Yasheng Gao for assistance with microscopy. This work was funded by NIH/NIGMS grant R35GM122488 to D.J.L.

REFERENCES

Altamirano S, Li Z, Fu M, Ding M, Fulton S, Yoder J, Tran V, Nielsen K (2021). The cyclin cln1 controls polyploid titan cells formation following a stress-induced G (2) arrest in Cryptococcus. mBio 12, e02509-21.

Aoki K, Hayashi H, Furuya K, Sato M, Takagi T, Osumi M, Kimura A, Niki H (2011). Breakage of the nuclear envelope by an extending mitotic nucleus occurs during anaphase in Schizosaccharomyces japonicus. Gene Cells 16, 911–926.

Berman J (2006). Morphogenesis and cell cycle progression in Candida albicans. Curr Opin Microbiol 9, 595–601.

Botstein D, Fink G (2011). Yeast: an experimental organism for 21st century biology. Genetics 189, 695–704.

Bundock P, den Dulk-Ras A, Beijersbergen A, Hooykaas P (1995). Trans-kingdom T-DNA transfer from Agrobacterium tumefaciens to Saccharomyces cerevisiae. EMBO J 14, 3206–3214.

Chater K, Chandra G (2008). The use of the rare UUA codon to define "Expression Space" for genes involved in secondary metabolism, development and environmental adaptation in Streptomyces. Microbiol 46, 1–11.

Chiou J, Balasubramanian M, Lew D (2017). Cell polarity in yeast. Annu Rev Cell Dev Biol, 33, 77–101.

Cheng K, Demirci A, Catchmark J (2011). Pullulan: biosynthesis, production, and applications. Appl Microbiol Biotechnol 92, 29–44.

Cock P, Antao T, Chang J, Chapman B, Cox C, Dalke A, Friedberg I, Hamelryck T, Kauff F, Wilczynski B, de Hoon M (2009). Biopython: freely available Python tools for computational molecular biology and bioinformatics. Bioinform 25, 1422–1423.

Cooke W (1959). An ecological life history of Aureobasidium pullulans (De Bary) Arnaud. Mycopathologia et Mycologia Applicata 12, 1–45.

Courtemanche N, Pollard T, Chen Q (2016). Avoiding artefacts when counting polymerized actin in live cells with LifeAct fused to fluorescent proteins. Nat Cell Biol 18, 676–683.

De Souza C, Osmani A, Hashmi S, Osmani S (2004). Partial nuclear pore complex disassembly during closed mitosis in Aspergillus nidulans. Curr Biol 14, 1973–1984.

Durandau E, Aymoz D, Pelet S (2015). Dynamic single cell measurements of kinase activity by synthetic kinase activity relocation sensors. BMC Biol 13, 55.

Gelvin S (2003). Agrobacterium-mediated plant transformation: the biology behind the "gene-jockeying" tool. Microbiol Mol Biol Rev 67, 16–37.

Gerstein AC, Fu MS, Mukaremera L, Li Z, Ormerod KL, Fraser JA, Berman J, Nielsen K (2015). Polyploid titan cells produce haploid and aneuploid progeny to promote stress adaptation. mBio 6, e01340-15.

Gladfelter A, Pringle J, Lew D (2001). The septin cortex at the yeast mother-bud neck. Curr Opin Microbiol 4, 681–689.

Gladfelter A (2015). How nontraditional model systems can save us. Mol Biol Cell 26, 3687–3689.

Goshima G (2022). Growth and division mode plasticity is dependent on cell density in marine-derived black yeasts. Genes Cells 27, 124–137.

Gostinčar C, Grube M, Gunde-Cimerman N (2011). Evolution of fungal pathogens in domestic environments? Fungal Biol 115, 1008–1018.

Gostinčar C, Ohm R, Kogej T, Sonjak S, Turk M, Zajc J, Zalar P, Grube M, Sun H, Han J, *et al*. (2014). Genome sequencing or four Aureobasidium pullulans varieties: biotechnological potential, stress tolerance, and description of new species. BMC Genomics 15, 549.

Gostinčar C, Turk M, Zajc J, Gunde-Cimerman N (2019). Fifty Aureobasidium pullulans genomes reveal a recombining polyextremotolerant generalist. Environ Microbiol 21, 3638–3652.

Grandi P, Doye V, Hurt E (1993). Purification of NSP1 reveals complex formation with 'GLFG' nucleoporins and a novel nuclear pore protein NIC96. EMBO J 12, 3061–3071.

Guo J, Wang Y, Li B, Huang S, Chen Y, Guo X, Xiao D (2017). Development of a one-step gene knock-out and knock-in method for metabolic engineering of Aureobasidium pullulans. J Biotechnol 251, 145–150.

Hooykaas P, Roobol C, Schilperoort R (1979). Regulation of the transfer of TI plasmids of Agrobacterium tumefaciens. Microbiol 110, 99–109.

Howell A, Lew D (2012). Morphogenesis and the cell cycle. Genetics 190, 51–77.

Hunter J (2007). Matplotlib: A 2D graphics environment. Computing in Science & Engineering 9, 90–95.

Ianiri G, Boyce K, Idnrum A (2017). Isolation of conditional mutations in genes essential for viability of Cryptococcus neoformans. Curr Genet 63, 519–530.

Idnurm A, Bailey A, Cairns T, Elliott C, Foster G, Ianiri G, Jeon J (2017). A silver bullet in a golden age of functional genomics: the impact of Agrobacterium-mediated transformation of fungi. Fungal Biol Biotechnol 4, 6.

Konzack S, Rischitor P, Enke C, Fischer R (2005). The role of the kinesin motor KipA in microtubule organization and polarized growth of Aspergillus nidulans. Mol Biol Cell 16, 497–506.

Kopecka M, Gabriel M, Takeo K, Yamaguchi M, Svoboda A, Ohkusu M, Hata K, Yoshida S (2001). Microtubules and actin cytoskeleton in Cryptococcus neoformans compared with ascomycetous budding and fission yeasts. Eur J Cell Biol 80, 303–311.

Kozubowski L, Heitman J (2010). Septins enforce morphogenetic events during sexual reproduction and contribute to virulence in Cryptococcus neoformans. Mol Microbiol 75, 658–675.

Lichius A, Berepiki A, Read N (2011). Form follows function – the versatile fungal cytoskeleton. Fungal Biol 115, 518–540.

Lübbehüsen T, Nielsen J, McIntyre M (2003). Characterization of the mucor circinelloides life cycle by on-line image analysis. J Appl Microbiol 95, 1152–1160.

Mackinnon J, Vinelli H (1949). Observations on the multiple-budding form of Paracoccidioides brasiliensis in cultures. An Fac Med Montevideo 34, 461–470.

Medina E, Robinson K, Bellingham-Johnstun K, Ianiri G, Laplante C, Fritz-Laylin L, Buchler N (2020). Genetic transformation of Spizellomyces punctatus, a resource for studying chytrid biology and evolutionary cell biology. eLife 9, e52741.

Mitchison-Field L, Vargas-Muniz J, Stormo B, Vogt E, Van Dierdonck S, Pelletier J, Ehrlich C, Lew D, Field C, Gladfelter A (2019). Unconventional cell division cycles from marine-derived yeasts. Curr Biol 29, 3439–3456.

Onetto C, Schmidt S, Roach M, Borneman A (2020). Comparitive genome analysis proposes three new Aureobasidium species isolated from grape juice. FEMS Yeast Res 20, foaa052.
Parra M, Libkind D, Hittinger C, Álvarez L, Bellora N (2023). Assembly and comparative genome analysis of a Patagonian Aureobasidium pullulans isolate reveals unexpected intraspecific variation. Yeast 40, 197–213.
Prasongsuk S, Lotrakul P, Ali I, Bankeeree W, Punnapayak H (2018). The current status of Aureobasidium pullulans in biotechnology. Folia Microbiol 63, 129–140.
Ramos S, Acha I (1975). A vegetative cycle of Pullularia pullulans. Trans Br Mycol Soc 64, 129–135.
Riedl J, Crevenna A, Kessenbrock K, Yu J, Neukirchen D, Bista M, Bradke F, Jenne D, Holak T, Werb Z, *et al*. (2008). Lifeact: a versatile marker to visualize F-actin. Nat Methods 7, 605–607.
Russel J, Theriot J, Sood P, Marshall W, Landweber L, Fritz-Laylin L, Polka J, Oliferenko S, Gerbich T, Gladfelter A, *et al*. (2017). Non-model model organisms. BMC Biol 15, 55.
Sawin K, Lourenco P, Snaith H (2004). Microtubule nucleation at non-spindle pole body microtubule-organizing centers requires fission yeast centrosomin-related protein mod20p. Curr Biol 14, 763–775.
Schaffrath R, Breunig K (2000). Genetics and molecular physiology of the yeast Kluyveromyces lactis. Fungal Genet Biol, 30(3), 173–190.
Seviour R, Kristiansen B, Harvery L (1984). Morphology of Aureobasidium pullulans during polysaccharide elaboration. Transactions Br Mycol Soc 83, 350–356.
Sharp P, Li W (1987). The codon adaptation index –a measure of directional synonymous codon usage bias, and its potential applications. Nucleic acids res 15, 1281–1295.
Silov S, Zaburannyi N, Anisimova M, Ostash B (2021). The use of the rare TTA codon in Streptomyces genes: significance of the codon context? Indian J Microbiol 61, 24–30.
Slepecky R, Stramer W (2009). Phenotypic plasticity in fungi: a review with observations on Aureobasidium pullulans. Mycologia 101, 823–832.
Steinberg G, Perez-Martin J (2008). Ustilago maydis, a new fungal model system for cell biology. Trends Cell Biol 18, 61–67.
Straube A, Brill M, Oakley B, Horio T, Steinberg G (2003). Microtubule organization requires cell cycle-dependent nucleation at dispersed cytoplasmic sites: polar and perinuclear microtubule organizing centers in the plant pathogen Ustilago maydis. Mol Biol Cell 14, 642–657.
Sutradhar S, Yadav V, Sridhar S, Sreekumar L, Bhattacharyya D, Ghosh S, Paul R, Sanyal K (2015). A comprehensive model to predict mitotic division in budding yeasts. Mol Biol Cell 26, 3954–3965.
Theisen U, Straube A, Steinberg G (2008). Dynamic rearrangement of nucleoporins during fungal "open" mitosis. Mol Biol Cell 19, 1230–1240.
Tu G, Wang Y, Feng J, Li X, Guo M, Zou X (2015). Agrobacterium tumefaciens-mediated transformation of Aureobasidium pullulans and high-efficient screening for polymalic acid producing strain. Sheng Wu Gong Cheng Xue Bao 31, 1063–1072.
Ukil L, De Souza C, Liu H, Osmani S (2009). Nucleolar separation from chromosomes during Aspergillus nidulans mitosis can occur without spindle forces. Mol Biol Cell 20, 2132–2145.
Walther A, Wendland J (2003). Septation and cytokinesis in fungi. Fungal Genet Biol 40, 187–196.
Warenda A, Konopka J (2002). The septin function in Candida albicans morphogenesis. Mol Biol Cell, 13, 2732–2746.
Xiong L, Zeng Y, Tang R, Alper H, Bai F, Zhao X (2018). Condition-specific promoter activities in Saccharomyces cerevisiae. Microb Cell Fact 17, 58.
Yang S, Yeh E, Salmon E, Bloom K (1997). Identification of a mid-anaphase checkpoint in budding yeast. J Cell Bio 136, 345–354.
Zhang Y, Feng J, Wang P, Xia J, Li X, Zou X (2019). CRISPR/Cas9-mediated efficient genome editing via protoplast-based transformation in yeast-like fungus Aureobasidium pullulans. Gene 709, 8–16.